MSUCL-385
October 1982

Macroscopic model for low energy heavy ion collisions

G.F. Bertsch
Cyclotron Laboratory
and
Department of Physics
Michigan State University
East Lansing, MI 48824-1321

Abstract

We propose a simple model for heavy ion collisions, based on a small number of dynamic variables. In addition to the relative coordinate of the centers of mass of the two nuclei, we consider only one other geometric variable, the radius of a neck joining the two nuclei. It is then possible to formulate an equation of motion mimicking the TDHF dynamics. The deep inelastic scattering phenomenon is reproduced quite well with much of the energy loss going to surface energy of the separating nuclei. The fusion cross sections show a low-ℓ window, as in TDHF.

I. Introduction

There is a need for a simple heavy ion collision model which mimics the dynamics of Time-Dependent Hartree Fock theory (TDHF). We not only would like a better understanding of TDHF physics, but we would also like to have a framework to see features of the dynamics that lie beyond the scope of TDHF. To this end we propose a classical model in which only the most essential geometric variables are retained. We start with the relative coordinate between the two nuclear centers of mass. The dynamics based on this variable alone has been explored by Gross and Kalinowski.[1] This will be augmented by one additional geometric variable, related to the neck region joining the two nuclei. It might seem that the many shape degrees of freedom are necessary, but in fact their role in the dynamics is implicit and we do not need to deal with them directly. To see how this simplification comes about, consider two nuclei which have collided and are connected by a neck. We ask how the relative coordinate between the two centers of mass evolves in time. If we draw a plane through the neck region which divides the combined system into two parts with appropriate masses, then it is rigorously true that the acceleration of the relative coordinate is given by the force of the nucleons on one side acting on those on the other side, plus the momentum flux across the surface due to the nucleon flux,

$$\mu\ddot{\vec{r}} = -\int_a dr''\rho(r'') \int_b dr'\rho(r')\vec{\nabla}v(r''-r') + \int\tilde{\tau}\cdot dA \qquad (1)$$

with

$$\mu = m\frac{A_aA_b}{A_a+A_b} \quad .$$

Here the two sides are labeled by a and b, m is the nucleon mass, $\vec{r}$ is the relative coordinate, v(r) is the two body interaction, and $\tilde{\tau}$ is the momentum flux tensor.[2] When we go to a macroscopic description of the nuclei, the right hand side is replaced by the sum of three terms, a Coulomb force, a bulk nuclear force, and a surface tension:

$$\mu\ddot{\vec{r}} = \vec{F}_{coul} + \vec{F}_{bulk} + \vec{F}_{surface} \tag{2}$$

In mean field theory, these forces can be calculated as integrals over the single-particle density matrix. However, we shall use a much simpler description, expressing the force solely in terms of the separation of coordinate $\vec{r}$ and the radius of the neck joining the nuclei, r_{neck}. The functional form of the force is discussed in the next section. Following that, we set up a model for the evolution of r_{neck}, based on the results of TDHF calculations. In this respect our model differs from other classical descriptions in which an attempt is made to calculate the neck evolution dynamically.[3,4] We then compare the model predictions with TDHF and with the data. We find that the main qualitative features of TDHF are well reproduced. This includes the deep inelastic scattering phenomenon, and the behavior of fusion cross sections as a function of bombarding energy and the sizes of the colliding nuclei.

II. The Force

Of the three forces to be specified in Eq. (2) the surface force gives least difficulty; it is just the surface tension

multiplied by the circumference of the neck. In terms of the neck radius r_{neck}, and the surface tension σ, this is

$$\vec{F}_{surface} = r_{neck}\, 2\pi\sigma\, \hat{r} \tag{3}$$

where $\hat{r}$ is the unit vector in the radial direction. We take the surface tension from the empirical surface energy,

$$\sigma = \frac{b_{surface}}{4\pi r_0^2} \approx \frac{(17\ \text{MeV})}{4\pi(1.15\ \text{fm})^2} \approx 1.0\ \text{MeV/fm}^2 \tag{4}$$

This force should not be confused with the proximity force of Blocki, et al.[5] The proximity force is properly defined as a force between separated nuclei, while the force in Eq. (3) applies to the situation in which the nuclei have already fused together.

We next consider the bulk nuclear force, which we write as the integral of the bulk stress across the dividing plane:

$$\vec{F}_{bulk} = \int s \cdot dA \approx \tilde{\tilde{s}} \cdot \hat{r}\ \pi r_{neck}^2 \tag{5}$$

The stress tensor can in general be a complicated function of the previous history of the system.† However, to the extent that the neck region is small compared to the rest of the system, the stress tensor can be parameterized in terms of the bulk dynamics. In mean field theories such as TDHF, the stress has two components.[2,6] There is an isotropic component associated with the potential field, and a possibly anisotropic component associated with the momentum flux $\tilde{\tau}$ carried by the particles. The tangential force only arises

†For example, for a nucleus in equilibrium, there is a positive isotropic stress (pressure!) whose integral over a plane cutting the nucleus just balances the surface force from the edge.

from this component, and it may be evaluated as an integral of the Wigner function of the one-body density.[2] Taking the Fermi gas model for the one-body density, this yields Randrup's window formula,[7]

$$F_T = \frac{dn}{dt}\, m v_T^N \tag{6}$$

where

$$\frac{dn}{dt} = \frac{3}{16}\, \rho_0 v_F\, \pi r_{neck}^2 \tag{7}$$

is the one-sided flux of particles across the surface, evaluated in the Fermi gas model.† In Eq. (7), $\rho_0 \approx 0.16/fm^3$ is nuclear matter density and $v_F \approx 0.28c$ is the Fermi velocity. The quantity v_T^N is the relative tangential velocity of the Fermi surfaces on the two sides of the neck. This is equal to the relative velocities of the nuclear centers of mass providing the nuclei do not have any internal motion. When the nuclei have internal angular momentum the relative velocities of the surfaces are modified by the internal rotation of the nuclei. Specifically, we shall take the relative velocity at the surfaces to be

$$v_T^N = \dot{r}_T - \frac{R_a \ell_a}{I_a} - \frac{R_b \ell_b}{I_b} \tag{8}$$

where $\dot{r}_T$ is the tangential component of the relative velocity of the centers of mass. Here ℓ_i is the intrinsic angular momentum of one of the nuclei, I_i is its moment of inertia, and $R_i = 1.15\, A_i^{1/3}$ the nuclear density radius. The intrinsic angular momentum will be determined assuming that the torque on a nucleus is proportional

†In general, some caution is required in using the concept of one-sided flux, since it is not an observable quantity. We thank F. Stancu and L. Wilets for an interesting discussion on this point.

to its radius. Then angular momentum conservation yields

$$\ell_i = (\ell_{\text{initial}} - \mu r \dot{r}_T) \frac{R_i}{R_a + R_b} \tag{9}$$

In Eq. (8) we will take the moments of inertia to be those of ellipsoids with axes R_i and $rR_i/R_a + R_b$,

$$I_i = \frac{1}{5} A_i m R_i \left(1 + \left(\frac{r}{R_a + R_b}\right)^2\right) \tag{10}$$

This now determines the transverse force and the angular momentum transfer, given the relationship of the coordinates r and r_{neck}.

The longitudinal component of the stress is a much more subtle issue. To zeroth order in the relative velocity of the two Fermi spheres, the longitudinal stress vanishes.[2] In first order, there is a contribution from both the particle flux and the potential field. The importance of the potential field is not known a priori. Fortunately, we can obtain independent information about the bulk forces from the compressibility of nuclear matter, which is inferred from the energy systematics of the giant monopole vibration. It is found that the compressibility is close to that of a free Fermi gas, i.e. the potential field effects are small. Thus it seems reasonable to neglect the potential contribution to the longitudinal stress. In that case, the force reduces to the longitudinal part of Randrup's window formula,[7]

$$F_L = 2 \frac{dn}{dt} m v_L^N \tag{11}$$

This formula contains the relative longitudinal velocities of the two Fermi spheres v_L^N, which now needs to be specified. Randrup

assumes that the Fermi spheres have the same velocity as the centers-of-mass of the two nuclei, which reduces the force to a linear friction. However this assumption neglects important physics associated with the finite transit time of the nucleons across each nucleus.[8] The shape of the Fermi surface at the neck position is determined by the velocities of the nuclear surfaces at some earlier time, when the nucleons that have reached the neck region were being reflected from distant surfaces. The time delay implies that the longitudinal force is not dissipative on short time scales. For example, the memory of previous longitudinal motion can promote subsequent fission, which indeed takes place readily in TDHF. We note that this time delay is implicit in the model of heavy ion collisions based on surface vibrations;[18] here the characteristic time is of the order of a vibrational period. We shall take this physics into account by assuming that there is a time delay t_D relating to the longitudinal velocity of the Fermi surfaces to the velocity of the centers of mass. Also, the nucleons will slow down in traversing the nucleus due to the long range of the Coulomb force. We take these features of the mean field dynamics into account using the following function for v_L^N,

$$v_L^N(t) = \vec{v}_D \cdot \hat{r}(t) + \frac{Z_a Z_b e^2}{A_a m v_F} \left(\frac{1}{\lambda r(t) + R_a} - \frac{1}{\lambda r(t)} \right) \qquad (12)$$

where $$\vec{v}_D = \dot{r}_L(t - t_D)\hat{r}(t - t_0) + \dot{r}_T(t - t_0)\hat{n}(t - t_0)$$

and $\lambda = R_b/(R_a+R_b)$. The unit vector $\hat{n}$ is in the reaction plane and perpendicular to $\hat{r}$. The parameter t_0 is the transit time of nucleus a,

$$t_0 = \frac{2R_a}{v_F}$$

The time scale of the longitudinal

delay t_D is set by t_0. If the far surfaces of the nuclei moved with the same velocity as their centers of mass, t_D would equal t_0. However, there will also be some delay in the motion of the far surface with respect to the center of mass motion. In one-dimensional slab dynamics,[9] the memory time is twice t_0, with a sudden reversal in v_L^N occurring at that point. Since the memory function (12) is smooth, we compensate by choosing t_D somewhat smaller than twice the transit time,

$$t_D = 1.5\ t_0 \tag{14}$$

For collisions between nuclei of unequal size, we use the smaller time scale, taking nucleus a to be the smaller one. This now specifies the bulk force in terms of the geometric variables.

The third force to consider is the Coulomb force. A simple model would be to treat it as though all of the charges were concentrated at the centers of mass,

$$F_{coul} = \frac{Z_1 Z_2 e^2}{r^2} \tag{15}$$

However, this approximation underestimates the actual Coulomb force for the separating fragments by as much as 20%, and a more precise formula is needed. To this end we will treat the nucleus as two spheres joined by a cylinder, whose radius is r_{neck} and whose length is $s = r - R_a - R_b$. Then the Coulomb force is approximated by

$$F_c \cong e^2 \frac{(Z_z - Z_n)(Z_b - Z_n)}{(r_a + r_b)^2} + e \sum_i^2 \frac{(Z_i - Z_n) Z_n}{(r_i + \frac{s}{4})} e^2 \frac{Z_n^2}{(\frac{s}{2})^2 + \frac{r_{neck}^2}{4}} \tag{16a}$$

where

$$Z_n = \pi r_{neck}^2 \rho_z \frac{s}{2} \tag{16b}$$

and

$$r_i = \frac{Z_i (R_i + \frac{s}{2}) - Z_n \frac{s}{4}}{Z_i - Z_n} \tag{16c}$$

Finally, to accurately describe grazing collisions, it is important to include the interaction of the nuclei before they touch. The potential interaction at large distances is well known from elastic scattering and fusion cross section systematics. We will use the potential of Bass,[10]

$$V(r) = \frac{-R_a R_b}{R_a+R_b}\left(0.03\ e^{s/3.3} + .0061\ e^{s/.65}\right)^{-1} \qquad (17)$$

where $s = r - R_a^B - R_b^B$; $R_i^B = R_i - 1.39\ A_i^{-1/3}$

There is also particle transfer at large distances, due to nucleon tunnelling under the potential barrier. We will assume that this particle flux carries the same momentum as in eqs. (6) and (11). The particle tunnelling rate has been calculated by Ko, et al.,[11] and we adopt their parameterization,

$$\frac{dn}{dt} = \frac{2\pi R_a^v R_b^v}{R_a^v + R_b^v}\left(0.0142\ e^{-1.9Z} - .0060\ e^{-2.98Z}\right) \qquad (18)$$

where $Z = r - R_a^v - R_b^v$ and R_i^v is the potential radius, $R_i^v = 1.25\ A_i^{1/3}$.

III. Geometry of the Model

All that remains to completely specify the model is the description of the evolution of the neck radius r_{neck}. We first note that the dynamics are quite different when the centers of mass of the two nuclei approach each other ($\dot{r}_L < 0$) than when they rebound ($\dot{r}_L > 0$). The TDHF calculations[12] show that the motion of the nuclei in the approach phase is close to that of rigid spheres, with the overlap region of the spheres defining the neck size. The neck has a quick initial expansion from a very small radius,

and it only exceeds the geometric overlap size slightly at the closest approach point. We shall make a quantitative model for these considerations by defining a geometry of three touching circles, representing the two nuclei and a joining neck, as shown in Fig. 1. The neck radius in this geometry is

$$r_{neck} = \frac{\sqrt{(R_a+R_b+r+2c)(R_a-R_b+r)(R_b-R_z+r)(R_a+R_b+2c-r)} - c}{4r} \qquad (19)$$

and c is the radius of the joining circle. At the simplest level, we could take $c = 0$ as has been done by others.[8,13] However, the growth of the neck radius during the approach phase is partly due to the fact that nuclear matter flows to smooth out the neck region, increasing c. We will assume that this growth in c is a highly overdamped process, so the rate at which it changes is proportional to the force associated with that coordinate. The hydrodynamic pressure associated with the surface curvature is proportional to c^{-1}. Thus we shall assume that c evolves according to the equation

$$\dot{c} = \frac{\alpha}{c} \qquad (20)$$

The parameter α will be chosen to reproduce the TDHF results. The initial value of c is determined by requiring the neck to begin with zero radius at a definite time after the half-potential radii of the nuclei touch, $r \leq R_a + R_b$.

The rebound phase has completely different dynamics. This phase is several times as long as the approach phase, so hydrodynamic considerations are more likely to be relevant in describing the overall shape. Again, we assume that the motion is overdamped

so that the rate of neck shrinkage is proportional to some generalized force. Without going into any details of the dynamics, it seems reasonable that this force would be proportional to the rate at which the system was extending, $\frac{dr}{dt}$. We are thus led to parameterize the neck shrinkage as

$$\dot{r}_{neck} = -\beta \dot{r}_L \tag{21}$$

with β a phenomenological constant to be determined by comparison with TDHF calculations. The linear dependence of Eq. (21) turns out to be a remarkably good approximation, when compared with the TDHF calculations of Dhar and Nilsson[12] for $^{208}Pb + ^{208}Pb$. In their Fig. 4 they show a linear dependence between r_{neck} and r lasting up to the scission point. From these results we are able to complete the parameterization. The neck shrinkage rate is well described using $\beta = 1/3$ in Eq. (21). The onset of the neck in the calculation of Dhar and Nilsson occurs at $r = 14.3$ fm, which corresponds to a time delay of 9 fm/c from the time at which the nuclear potentials touch, $r = 14.8$ fm. Finally, the growth of the neck during the approach phase is fit with $\alpha = 0.04$ fm-c. The comparison of our model with Ref. 12 is shown in Fig. 2. The model agrees quite well with TDHF except for the closest approach points, where the TDHF predicts a larger neck than the model provides. We shall see that this deficiency is of no consequence for calculating energy losses, but is of some importance in determining the deflection function.

We next discuss the treatment of scission. The neck becomes hydrodynamically unstable if it is too narrow in relation to its

length,[14] and will pinch off spontaneously. However, fast hydrodynamic flow is possible only when the single particle wavefunctions are nodeless. Thus, the instability will cause a rapid scission when the neck radius falls to the alpha particle radius. In the present model, we assume scission to occur suddenly when $r_{neck} \leq$ 1 fm. Scission occurs in this fashion for the reaction of Fig. 2.

There is another mechanism for neck breakage when the nuclei rebound at high velocity. An instability develops with respect to density fluctuations when the bulk density falls below a critical value, of the order of 2/3 of nuclear matter density. According to Ref. 9, this happens in mean field theory in the bulk limit when the separation velocity exceeds 0.06 c. This separation mechanism we call the snapping of the neck, and we invoke it when either

$$\dot{r}_L > 0.06\ c \quad \text{or} \quad V_L^N > 0.06\ c\ . \tag{22}$$

IV. The Deep Inelastic Scattering Phenomenon

One of the most significant observables in heavy ion collisions is the energy loss spectrum, $\frac{d\sigma}{dE}$. In many cases there are two peaks in this spectrum, one for small energy losses, the quasielastic scattering, and one for large energy losses, the deep inelastic scattering. It seems to be quite difficult to obtain a low energy peak in simple classical models, even in models that overlay statistical transport effects on the classical dynamics. In contrast, in our model the deep inelastic peak arises quite naturally as the energy cost of stretching out the

fused nuclei into an extended system with a long neck. To the extent that the geometry of this extended system is independent of the impact parameter, the energy loss will be independent also, and therefore give a sharp peak in the energy loss spectrum. This mechanism of the energy loss has been recognized for some time.[15] To examine it more quantitatively, we note that the energy loss due to surface tension can be expressed in terms of the work done by $F_{surface}$,

$$W_{surface} = \oint \vec{F}_{surface} \cdot d\vec{r} = 2\pi\sigma \oint r_{neck}\, dr \qquad (23)$$

Since it is only the area that counts here, the inner part of the motion which followed a reversible path does not contribute to the energy loss. For a rough estimate, we can make a triangular approximation for the dependence of r_{neck} on r,

$$W_{surface} = 2\pi\sigma \int_{r_{neck(max)}} r_{neck}\, dr = \frac{\pi\sigma}{\beta} \left(r^2_{neck(max)} - 1\right) \qquad (24)$$

For the $^{208}Pb + ^{208}Pb$ collision, we have $r_{neck(max)} \approx 4.5$ fm and

$$W_{surface} \approx \frac{\pi(1\ MeV/fm^2)}{1/3} (4.5\ fm)^2 \approx 180\ MeV \qquad (25)$$

The loss of surface in the approach phase contributed 40 MeV to the energy in the relative coordinate, leaving a net energy loss of 140 MeV. This is roughly half of the total energy loss in the collision. The remaining part of the energy loss is the dissipative component of the bulk force, Eqs. (6) and (11). This result is important for consideration of statistical effects during the collision. Since much of the energy loss is contained in

deformation energy, it is not available as thermal energy for such statistical processes as prompt particle emission, etc.

We now examine the dependence of the energy loss on impact parameter. The maximum neck radius is rather insensitive to the impact parameter, as may be seen from the example in Fig. 3, the collision of $^{84}Kr + ^{209}Bi$, at $E_{cm} = 428$ MeV. Consequently, the surface energy loss does not depend strongly on impact parameter. Furthermore, the tangential force causes an energy loss which increases with impact parameter, so the net energy loss is rather flat. The total energy loss calculated for the $^{84}Kr + ^{209}Bi$ collision is shown in Fig. 4, compared with the TDHF calculation.[16] Small impact parameters are well described but the model predicts somewhat too little energy loss at larger impact parameters. The comparison of the experimental energy loss spectrum and the model prediction is shown in Fig. 5. We see that the model correctly reproduces the average energy loss in the deep inelastic peak, but it overestimates the prominence of that peak. This is of course to be expected; statistical transport effects will broaden any sharp structures of the classical model.

While the model gives a reasonable account of the quasielastic cross section, it appears to give too small a cross section for medium energy losses. This is not surprising, because the model does not take into account the deformation degrees of freedom before the nuclei touch. As has been emphasized by Broglia,[18] these degrees of freedom are very important for absorbing energy in grazing trajectories. The present model only allows energy loss at the larger distances via the particle transfer. In

particular, the tangential momentum transfer is responsible for all of the energy loss at large impact parameters.

V. Angular Momentum Transfer

The TDHF theory exhibits a rapid angular momentum transfer between target and projectile. The system approaches an equilibrium in which the angular momentum is shared between the relative motion and internal rotation in the same way as if the system were rotating rigidly. It appears that the transverse force associated with particle transfer is mostly responsible for this behavior. The dependence of the transverse force on the relative velocities of the Fermi spheres, Eq. (6), leads to an equilibrium of rigid rotation. That the rate of angular momentum transfer is large enough to establish equilibrium is a consequence of the large neck size, and the long duration of the collision on the time scale of t_0. Essentially, the criterion for equilibration is that the number of particles transferred be of the same magnitude as the number of nucleons in the system. This condition is met for low energy collisions.

As a specific example, we examine the collision of $^{238}U + ^{238}U$ at 7.5 MeV/n, which was studied in TDHFB theory by Cusson, et al.[19] The time evolution of the angular momentum is shown in Fig. 6, compared with the present model. Both calculations show a rapid approach to equilibrium. It is interesting to note that the TDHFB theory exhibits a slight overshoot, showing that there are memory effects in the transverse force, analogous to the

delayed response in the longitudinal force. This could be incorporated in the classical model in the same way as we did for the longitudinal force. However we feel that the effect on the dynamics is not important, and thus the added complication is not warranted.

In Table I we show the final angular momentum fraction of the TDHFB theory compared to the present calculation. The TDHFB theory gives slightly larger angular momentum transfer than the classical model. The equilibrium fraction for touching spheres may be easily derived from Eq. (6), setting $v_T = 0$, and is

$$L_{eq}/L_{initial} = \frac{5}{7} \quad . \tag{26}$$

Comparing with Table I, we see that equilibrium is not quite reached.

The potential field will also contribute to angular momentum transfer, and this is neglected in our model. There will be a torque exerted on the nuclei if the potential field is not symmetric under reflection through the plane defined by $\hat{n}$. This symmetry is approximately satisfied in TDHF, judging by the published figures of the density distributions in the reaction plane, e.g. Fig. 1 of Ref. 19. The potential field has been considered alone as a mechanism for angular momentum transfer,[20] and it was found that the system would come close to angular momentum equilibrium only if the particle transfer angular momentum was included in the calculation. Also, in the statistical transport description of heavy ion collisions, the particle transfer is more important than the potential field for angular momentum transfer.[21]

VI. Fusion Cross Sections

The fusion cross section is an important observable in the theory of heavy ion collisions. For a given energy and impact parameter, we consider the system to have fused if in the rebound phase the rebound velocity decreases to zero and becomes negative again. It is possible, both in our model and in TDHF, for the system to come apart in subsequent cycles of oscillation, but we feel that these would probably be damped out in a more realistic model of the dynamics. The fusion region predicted for the system $^{28}Si + ^{28}Si$ is shown in Fig. 7. The region with the outer boundary is the prediction of our classical model, and the inner region is the result of TDHF theory.[22] In both cases, the fusion region is bounded by three curves, with distinct physical mechanisms giving rise to the boundary. The low energy boundary is determined by the condition that the nuclei touch--once this happens, the nuclear force prevents the nuclei from separating again. The precise position of the contact curve depends only on the potential field dynamics for large separations of the nuclei. Given a good description of this potential field, the boundary should be accurately predicted. Both TDHF and the present model agree here, indicating that the Bass potential we used is close to the effective potential of TDHF theory.

It is commonplace to parameterize the fusion cross section in the threshold region by the critical distance formula,

$$b(E) = R_c\sqrt{1 - V_B/E} \tag{27}$$

In our model, the critical distance R_c is the top of the potential

barrier. At threshold with the Bass potential, the critical distance is 9.25 fm for the collision system of Fig. 7. The barrier top moves to smaller radii as the energy increases; at 75 MeV the barrier radius is reduced to 7.9 fm. Thus, the simple formula (27) is only correct to ∿15%, or ∿30% for cross sections.

The second boundary, at high energy and large impact parameter, is marked scission in Fig. 7. On this boundary, the nuclei have touched and formed a neck, and the nuclear force just balances the centrifugal and Coulomb repulsion. It is common to parameterize this boundary in terms of a critical angular momentum. For the TDHF calculation,[22] the boundary is at a constant angular momentum, with $\ell_c \sim 50\ \hbar$. At $E_{cm} = 100$ MeV, our classical model has a critical angular momentum 10% higher, $\ell_c \sim 55\ \hbar$. This discrepancy is not unexpected; there is a delicate balancing of forces and our parameterization is certainly not reliable below the 10% level. However, our model also predicts that the critical ℓ should increase with energy--at $E_{cm} = 150$ MeV, the model predicts $\ell_c \sim 59\ \hbar$. The reason for the increase is quite simple. The closest approach point has a larger neck radius for higher bombarding energies. The nuclear force will be stronger with a larger necking, giving a higher critical angular momentum.

When one considers heavier systems with higher charge, the Coulomb force becomes more important in determining the scission boundary until finally a point is reached at which the low energy fusion is cut off by the subsequent scission. For identical targets and projectiles, our model predicts this point to be

reached in the vicinity of $^{120}_{50}Sn$. The fusion region for the $^{120}Sn + ^{120}Sn$ system is shown in Fig. 8. We see that the fusion threshold is given by scission boundary, which extends down to $E_{cm} = 291$ MeV. The reaction threshold coincides with the boundary for touching, which begins at $E_{cm} = 264$ MeV. Evidently, for this system fusion requires an "extra push" as discussed by Swiatecki.[3]

The third boundary of the fusion region, at high energy, is labelled "neck snap" in Figs. 7 and 8. Above this point, the tensile strength of nuclear matter is exceeded, and the system comes apart without the neck necessarily shrinking smoothly to small radius. We see from Fig.7 that the TDHF threshold is substantially lower than the result of our model. There are two possible reasons for this. Our neck parameterization probably has too small a size for the closest collisions (cf. Fig. 2). With a larger neck, there would be more momentum transfer and the threshold would be more easily reached. The other possibility is that the tensile strength assumed in our model is too high. We chose $v_c = 0.06$ to reproduce the bulk dynamics in the mean field approximation.[9] This corresponds to a tensile strength of nuclear matter of

$$S_{max} = 1 \text{ MeV/fm}^3 \tag{28}$$

However, the one-dimensional TDHF calculations of finite systems indicate that nuclear matter is somewhat more fragile. Wong has argued that the critical velocity should be correspondingly small.[23] Obviously, this point needs further investigation. Unfortunately for our model, the critical velocity cannot be reduced from 0.06 c without causing a region of high impact parameters to be unstable against the neck snapping.[26]

VII. Deflection Functions

The quasielastic collisions scatter to an angle characteristic of grazing Coulomb trajectories. For light systems the closer collisions are scattered to more forward angles, because the attractive nuclear forces dominate at small distances. We illustrate this with the deflection function for $^{40}Ca + ^{40}Ca$ collisions at $E_{cm} = 139$ MeV. Table II shows the deflection as for various initial angular momenta, comparing TDHF (Ref. 24) with our model. The $\ell = 90$ ħ trajectory is nearly a grazing collision, and the deflection angle is close to the Coulomb deflection. The deflection becomes more forward for closer collisions, and is at negative angles for $\ell = 75$ ħ. At $\ell = 70$ ħ, the system fuses both in our model and in TDHF. The TDHF theory also has a fusion window below $\ell = 26$ ħ, but in our model the window does occur at such low energies.

When collision conditions permit fusion, it is obvious that the larger impact parameters have forward deflections, leading to negative angle scattering. Conversely, when the system has too high a charge to fuse, the deflection is backward for the close collisions. But in the lighter nonfusing systems, the deflection at intermediate impact parameters depends quite sensitively on the balance of forces. In TDHF, forward deflections are possible for nonfusing systems. This is illustrated in Fig. 9, showing the Wilczynski plots of the $^{84}Kr + ^{209}Bi$ collision at $E_{cm} = 428$ MeV. The TDHF shows a forward deflection of 10°-20° for mid range impact parameters, and a backward deflection for small impact parameters. Our model has the same qualitative behavior, but does

not show as dramatic a forward deflection for the mid range compact parameters. The agreement between the TDHF deflection function and the one we calculate would be better if the neck parameterization were improved to properly describe the thicker neck at small distances. More forward deflections are also obtainable by decreasing the memory time t_D, since a long membory time implies that the system bounces more elastically. We show this with the dashed line in Fig. 9, which is calculated with zero memory time and with the Coulomb acceleration in Eq. (12) reduced by half.

Finally, in the heaviest systems, the Coulomb force completely dominates the physics, and the forward deflections from the Coulomb trajectory are quite small. This is illustrated with Table III, comparing the deflection functions for $^{238}U + ^{238}U$ at $E_{cm} = 892$ MeV. The present model gives a result very close to the Coulomb trajectory, while the TDHFB theory gives a forward deflection of 5°-10°. The disagreement here may be partially due to the different physics with pairing included in TDHFB. Pairing makes the Fermi surface more spherical, which makes the system behave closer to hydrodynamics. There is no rebound in hydrodynamics, and the sticking is longer. We thus expect somewhat more forward deflections for TDHFB than TDHF.

VIII. Conclusion

We have set up a classical model for heavy ion collisions based on the known bulk dynamics of mean field theory. With a purely frictional particle transfer force it is not possible to reproduce qualitative features of the TDHF fusion cross sections,[24] and our model gives this force some nondissipative character via a memory time.[8] Conversely, our potential interaction includes a

surface force which has a dissipative part, due to the exit shapes being different from the entry shapes. The qualitative agreement of the model predictions with TDHF is quite good, so we feel this model should be a useful one in future studies of heavy ion reactions. The model is capable of reproducing such interesting features of TDHF as the deep inelastic scattering and the fusion window. Quantitatively, the model is not completely successful; details of the deflection function and of the high energy fusion boundary still elude us. Considering the parameters in the model as adjustable in the light of the data, undoubtedly a better description would result. However, our intent is to use the freedom of parameterization as a guide to go beyond the TDHF dynamics. For example, the observables depend quite strongly on the memory time t_D, and this parameter will be different in TDHF and a more complete theory.

The model could also be used to make a description of the statistical spreading that takes place during collision. The classical forces would be generalized to include the fluctuating components, which arise from quantum effects and from finite temperatures. It would then be possible to compute double differential cross sections which could compare directly with experiment.

IX. Acknowledgment

The author acknowledges helpful discussions with A. Dhar, F. Stancu, N. Takigawa, and P. Siemens. This work was supported by the National Science Foundation under grant PHY80-17605.

Table I. Angular momentum transfer in $^{238}U + ^{238}U$ at $E_{cm} = 892.5$ MeV. The ratio $R = \ell_{final}/\ell_{initial}$ is calculated at two impact parameters.

Initial angular momentum ℓ_i	R		
	TDHFB (Ref. 18)	Present model	Eq. 23
300	0.70	0.74	0.71
150	0.69	0.72	0.71

Table II. Deflection function for $^{40}Ca + ^{40}Ca$ at $E_{cm} = 139$ MeV

Initial ℓ (h)	Deflection Angle		
	TDHF (Ref. 21)	Present model	Coulomb
90	25°	22°	30°
80	-57°	2°	
75	-109°	-131°	
70	fuse	fuse	

Table III. Deflection function for $^{238}U + ^{238}U$ at $E_{cm} = 892$ MeV

b	Deflection Angle		
	TDHFB (Ref. 19)	Present model	Coulomb
2.09	141°	146°	146°
4.18	105°	115°	117°

References

1. D. Gross and H. Kalinowski, Phys. Reports 45 (1978) 175.
2. G. Bertsch, Nuclear Physics with Heavy Ions and Mesons, ed. Balian, et al., North-Holland, 1978, 239.
3. W. Swiatecki, Physica Scripta 24 (1981) 113.
4. J. Blocki, et al., Phys. Lett. 99B (1981) 13.
5. J. Blocki, J. Randrup, W.J. Swiatecki and C.F. Tsang, Ann. Phys. 105 (1977) 427.
6. A.A. Abriksov and I.M Khalatnikov, Reports on Progress in Physics 22 (1959) 336, eq. (6.3).
7. J. Randrup, Ann. Phys. 112 (1978) 356.
8. A. Jain and N. Sarma, Phys. Rev. C24 (1981) 1066.
9. G. Bertsch and D. Mundinger, Phys. Rev. C17 (1978) 1646.
10. R. Bass, Phys. Rev. Lett. 39 (1977) 265.
11. C.M. Ko, et al., Phys. Lett. 77B (1978) 174.
12. A. Dhar and B. Nilsson, Phys. Lett. 77B (1978) 50.
13. F. Beck, et al., Phys. Lett. 76B (1978) 35.
14. Rayleigh, Collected Scientific Papers, vol. I, (Dover, 1964), 361.
15. H. Morinaga, Proceedings of the Conference on Macroscopic Features of Heavy Ion Collisions, Hakone, 1977, p. 352.
16. K. Davies, et al., Phys. Rev. Letters 41 (1978) 632.
17. J.R. Huizenga, et al., Phys. Rev. Lett. 37 (1976) 885.
18. R.A. Broglia, et al., Phys. Lett. 61B (1976) 113.
19. R. Cusson, et al., Z. Phys. A294 (1980) 257.
20. R.A. Broglia, et al., Phys. Rev. Lett. 41 (1978) 25.
21. S. Shlomo, et al., Phys. Rev. C20 (1979) 1.

22. P. Bonche, et al., Phys. Rev. C20 (1979) 641.

23. C.Y. Wong, Phys. Rev. C25 (1982) 1460.

24. H. Flocard and M.S. Weiss, Phys. Rev. C18 (1978) 573.

25. D. Brink and F. Stancu, Phys. Rev. C24 (1981) 144.

26. D. Cha, private communication.

Figure Captions

Fig. 1 - The geometry specifying the neck radius in the approach phase of a heavy ion collision. The radii R_a R_b are half density radii of the nuclei, r is the separation of the two nuclear centers of mass, and c is the radius of a joining circle.

Fig. 2 - Relationship between neck radius r_{neck} and separation distance r for $^{208}Pb + ^{208}Pb$ at 800 MeV c.m. energy and zero impact parameter. The solid line is the present model, and the dashed line is from Ref. 12.

Fig. 3 - Maximum neck radius as a function of impact parameter, for the collision $^{84}Kr + ^{209}Bi$, calculated in the present model for $E_{cm} = 428$ MeV.

Fig. 4 - Final state energy in the collision $^{84}Kr + ^{209}Bi$, as a function of incoming angular momentum. Solid line is the present calculation, and triangles are the result of the TDHF calculation of Davies, et al., Ref. 16. The break in the solid curve is an unphysical discontinuity occurring when the nuclei just touch.

Fig. 5 - The energy loss spectrum for the collision $^{84}Kr + ^{209}Bi$ at $E_{cm} = 508$ MeV. The histogram is the experimental data of Huizenga, et al., Ref. 17. The curve is the result of the present model.

Fig. 6 - Angular momentum in the relative coordinate of $^{238}U + ^{238}U$ at $E_{cm} = 892.5$ MeV. The solid line is the present model, and the dashed line is the TDHFB calculation of Ref. 19. Time is measured from the point $r = 18.6$ fm.

Fig. 7 - Behavior of $^{28}Si + ^{28}Si$ collisions as a function of impact parameter and initial cm energy. The outer boundary shows the fusion region in the present model. The TDHF prediction[22] is shown in the heavy stipple.

Fig. 8 - Behavior of $^{120}Sn + ^{120}Sn$ collisions as a function of impact parameter and initial cm energy. The fusion region is shown in stipple. The area between the scission line and the contact line is the deep inelastic scattering region.

Fig. 9 - The deflection angle and final kinetic energy of the system $^{84}Kr + ^{209}Bi$, for initial energy $E_{cm} = 428$ MeV. The line is the prediction of the present model, with points labelled by the angular momentum ($\hbar$). The triangles are the results of TDHF theory.[16] The dashed line shows the present model with two parameter changes: the time delay t_D is set to zero and the Coulomb deceleration in Eq. (12) is reduced by half.

Appendix Fortran program for the collision model

```
c   TDHF-motivated classical collision model, by G. Bertsch
      integer stage,td
      real m,ml2,l,li
      dimension vrt(100),d(8)
     equivalence (zl,d(1)),(z2,d(2)),(al,d(3)),(a2,d(4)),(ecm,d(5)),
    1(ra,d(6)),(b,d(7))
     data m,hbar,rz,vsnap,d/931,197.3,0,.06,36,83,84,209,428,18,5,20/
   1  accept*,n          !see equivalence statement for parameter
      if(n.eq.0) go to 2 !                              assignment
        if(n.lt.0) stop
        if(n.le.8) accept*,d(n)
        if(n.le.8) print*,n,d(n)
        go to 1
   2  rl=1.15*al**.3333           !initialize the collision
      r2=1.15*a2**.3333
      rz=0.
      r=ra
      nstep=d(8)
      rbass=1.0087*(rl+r2)-1.598*(1./rl+1./r2)
      rpot=1.087*(rl+r2)
      z2e2=zl*z2*1.44
      ml2=m*al*a2/(al+a2)
      li=b*sqrt(2*ecm*ml2)/hbar
      epsilon=sqrt(l.+(2*ecm*b/z2e2)**2)
      temp=(l.+2*ecm*b**2/z2e2/r)/epsilon
      if(temp.lt.l.00001) go to 3
        print*,'unphysical initial conditions'
        go to 1
   3  theta=acos(-temp)-acos(-l./epsilon)
      x=r*cos(theta)
      y=r*sin(theta)
      vt=li*hbar/ml2/r
      vr=-sqrt(2.*(ecm-z2e2/r)/ml2-vt**2)
      vx=(vr*x-vt*y)/r
      vy=(vr*y+vt*x)/r
      td=3.*rl/0.28
      do 4 i=l,td
   4  vrt(i)=vr
      t=0
      stage=l
      nt=0
      k=l
   5  accept*,n
      if(n.ne.0) go to 1   ! carry the collision through several
      do 20 i=l,nstep      !               time steps
      t=t+l
      x=x+vx
      y=y+vy
      r=sqrt(x**2+y**2)
      k=k+l
      if(k.gt.td) k=l
      th3=atan(vt*td*.67/r)
      vrl=vrt(k)*cos(th3)+vt*sin(th3)
      rxl=r*r2/(rl+r2)
```

```
      if(rx1.lt.Ø.75*r2) rx1=Ø.75*r2
      vr2=-sqrt((-Ø.28+vr1)**2+2*z2e2/a1/m*(1./(rx1+r1)-1./rx1))+.28
      fc=z2e2/r**2
      z=r-rpot
      s1=r-r1-r2
      go to (6,6,8,9,1Ø), stage          !stage of collision
 6      if(z.lt.Ø) stage=2               ! 1:  before touching
        if(s1.lt.Ø) stage=3
        s=amin1(r-rbass,1Ø.)
        e1=exp(s/3.3)
        e2=exp(s/.65)
        fn=-r1*r2*(.ØØ9Ø9*e1+.ØØ938*e2)/(.Ø3*e1+.ØØ61*e2)**2/(r1+r2)
        fn=1.Ø87*fn
        vr1=vr
        dndt=7.42*r1*r2*(.Ø142*exp(-1.9*z)-.ØØ6*exp(-2.98*z))/rpot
        go to (15,7,15,1), stage
 7          nt=nt+1
            if(nt.gt.9) stage=3
            go to 15
 8    ry=amax1((r-r1-r2)/2.+.1,.1)     ! 3:  contact made here
        stage=4
 9    if(vr.gt.Ø) stage=5               ! 4:  nuclei approaching
        ss=(r1+r2+r+2*ry)*(r1+r2+2*ry-r)*(r+r1-r2)*(r+r2-r1)/4.
        rz=sqrt(ss)/r-ry
        ry=ry+.Ø4/ry
        go to 14
1Ø    rz=rz-.33*vr                     ! 5:  nuclei rebounding
        if(rz.lt.1.Ø) go to 23
        if(vr.gt.vsnap.or.vr1.gt.vsnap) go to 22
        if(vr.lt.Ø) go to 3Ø
        if(s1.le.Ø) go to 14
          zx=.Ø8*3.14*rz**2*s1/2        ! refined Coulomb force
          ra1=(-s1*zx/4.+z2*(r2+s1/2.))/(z2-zx)
          ra2=(-s1*zx/4.+z1*(r1+s1/2.))/(z1-zx)
          fc=1.44*((z1-zx)*(z2-zx)/(ra1+ra2)**2+(z1-zx)*zx/(ra1+s1/2)**2
     1    +(z2-zx)*zx/(ra2+s1/2)**2+zx**2/(s1**2/4.+rz**2/2.))
14    fn=-6.28*rz
        vr1=vr2
        dndt=.ØØ9*rz**2*3.14
15    fr=fn+fc-2*m*vr1*dndt             ! radial force
      fp=2*m*vr1*dndt
        finertia=(r1**2/a1/(r1**2+(r*r1/(r1+r2))**2)+r2**2/a2/(r2**2+
     1  (r*r2/(r1+r2))**2))*5./m/(r1+r2)
        ft=-(vt-(li-1)*hbar*finertia)*m*dndt  !tangential force
        vx=vx+(x*fr-y*ft)/m12/r
        vy=vy+(y*fr+x*ft)/m12/r              !Newton's equation
        vr=(vx*x+vy*y)/r
        vt=(-vx*y+vy*x)/r
        vrt(k)=vr
      l=m12*vt*r/hbar
2Ø    continue
      e=z2e2/r+m12*(vx**2+vy**2)/2.
      print112,t,r,rz,vr,vr1,l,e
112   format(8f1Ø.5)
      go to 5
22    print*,'neck snaps'
```

```
      go to 24
23    print*,'scission'
24    eps=sqrt(1.+(1*hbar/z2e2)**2*2*e/m12)
      thd=acos(-((1*hbar)**2/(m12*z2e2*r)+1)/eps)-acos(-1./eps)
      th1=atan(y/x)
      th2=atan(vy/vx)
      type*,x,y,th1,vx,vy,th2
      theta=90.-(atan(-x/y)+thd)*57.3
      print*,theta,1,e
      go to 1
30    print*,'fusion'
      go to 1
      end
```

MSUX-80-377

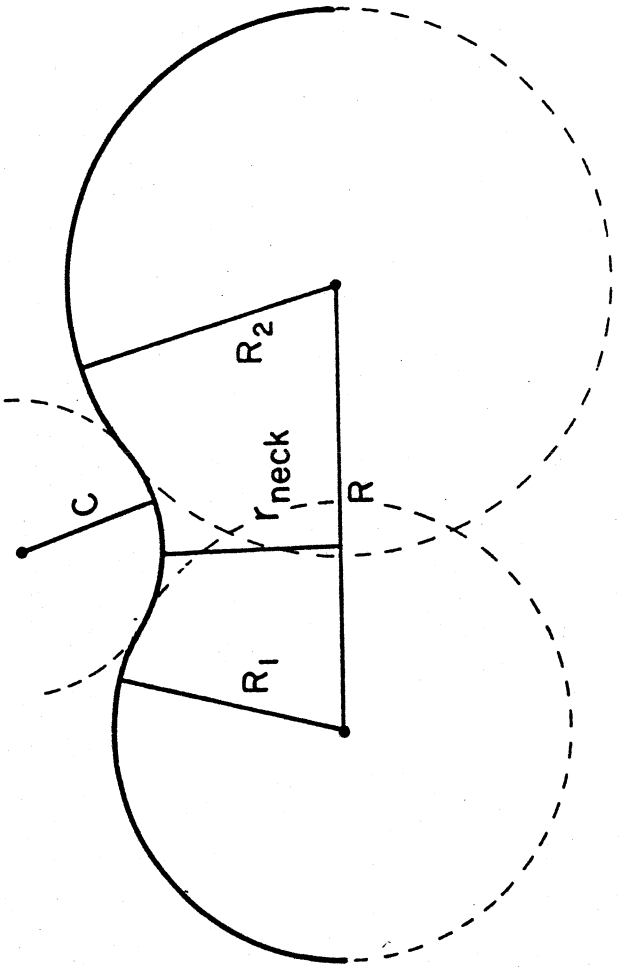

Figure 1

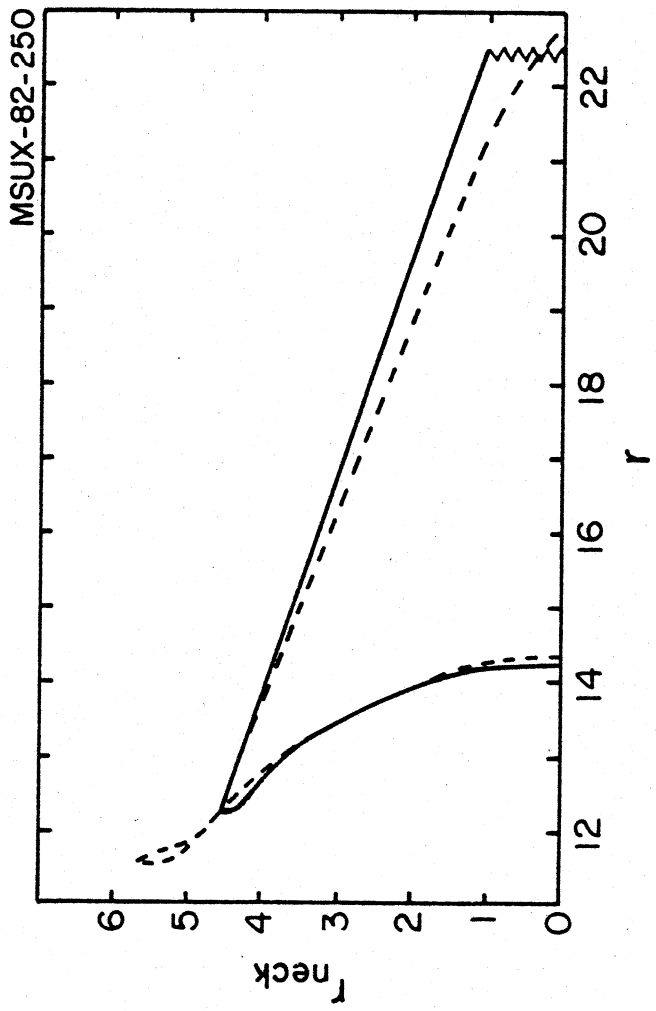

Figure 2

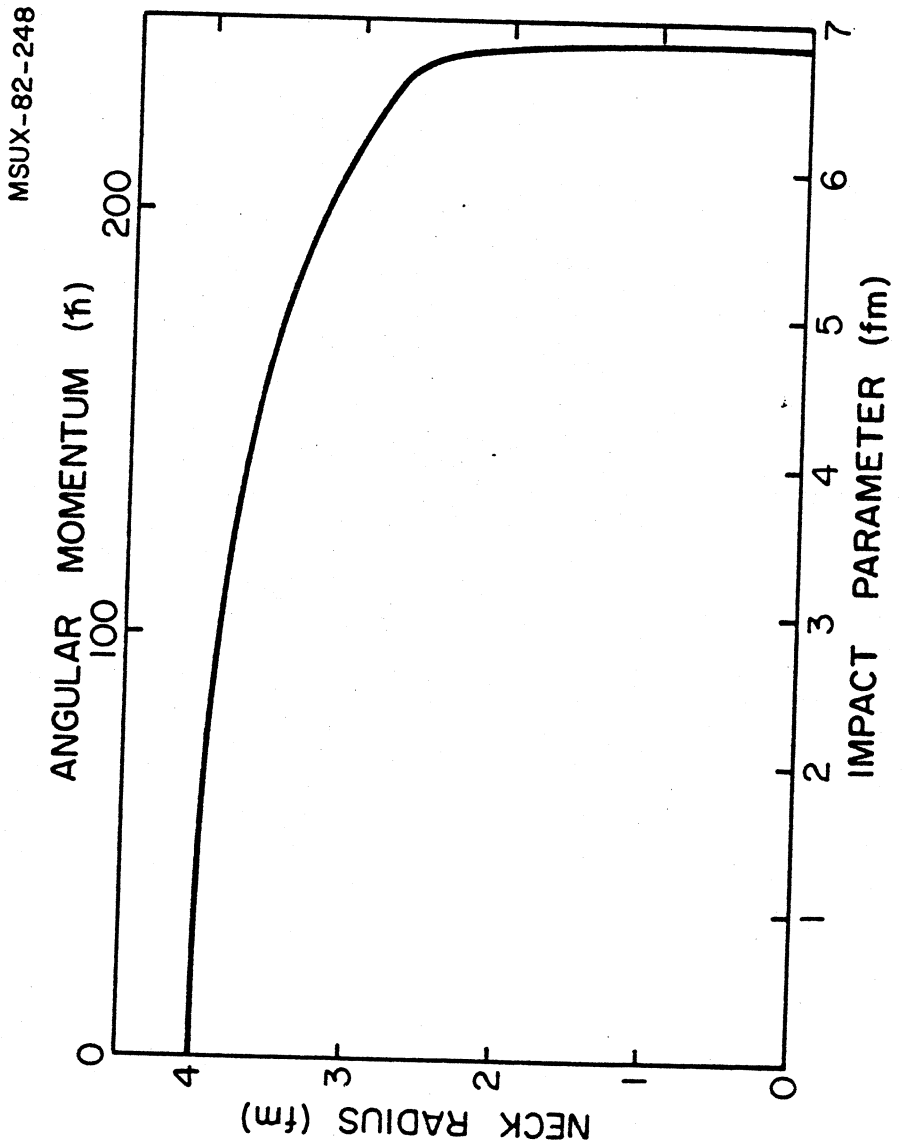
MSUX-82-248
ANGULAR MOMENTUM (ħ)
0
100
200
NECK RADIUS (fm)
0
1
2
3
4
IMPACT PARAMETER (fm)
0
1
2
3
4
5
6
7

Figure 3

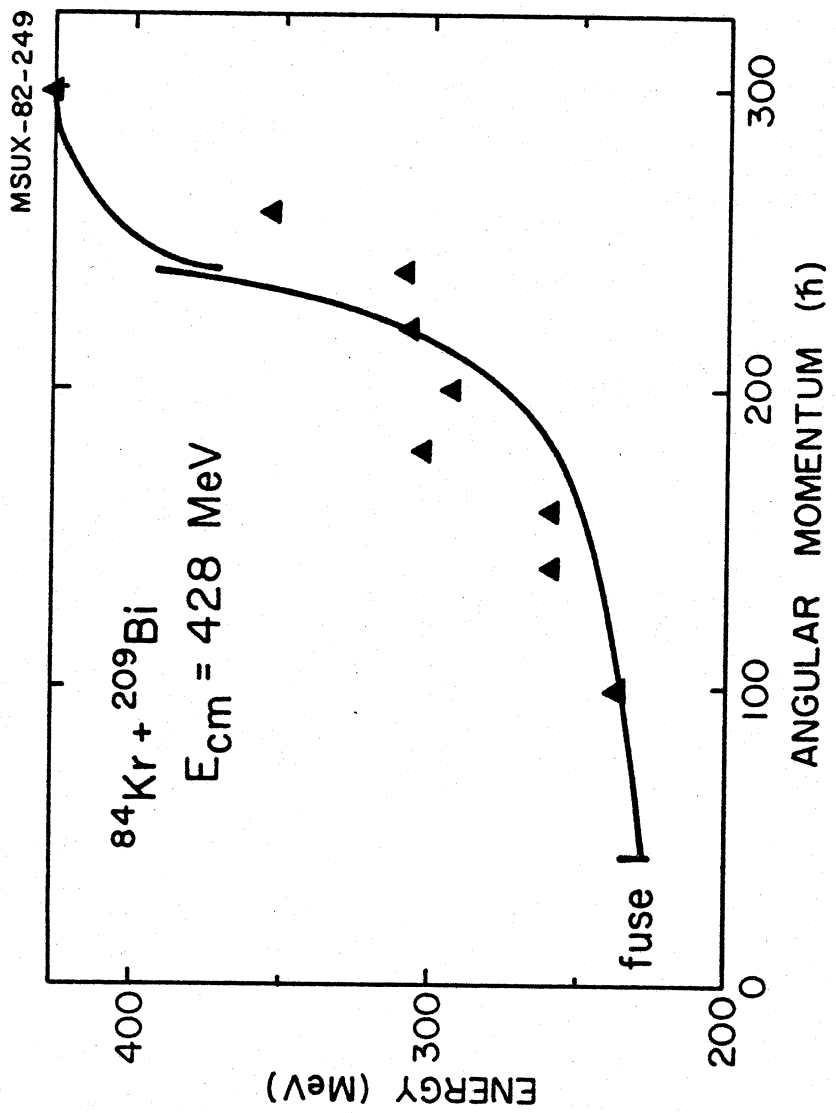
MSUX-82-249
$^{84}Kr + ^{209}Bi$
E_{cm} = 428 MeV
fuse
ENERGY (MeV)
400
300
200
0
100
200
300
ANGULAR MOMENTUM (ħ)

Figure 4

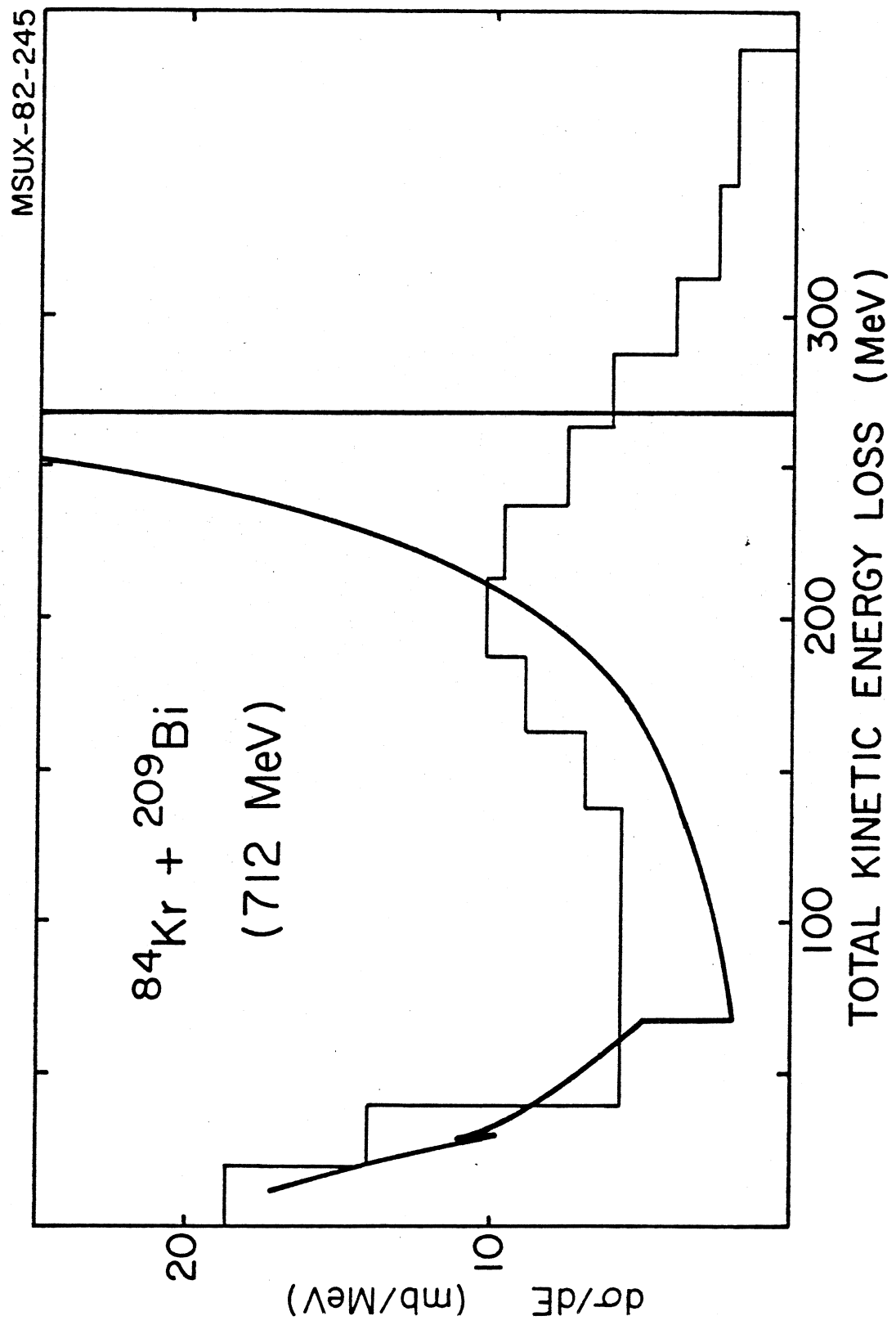
MSUX-82-245
$^{84}Kr + ^{209}Bi$
(712 MeV)
dσ/dE (mb/MeV)
20
10
100
200
300
TOTAL KINETIC ENERGY LOSS (MeV)

Figure 5

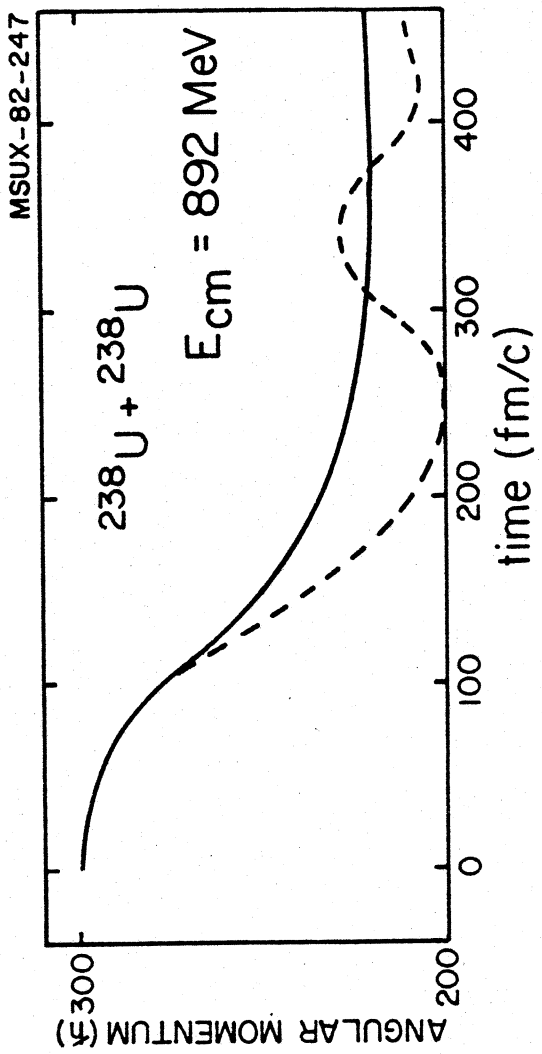
MSUX-82-247
$^{238}U + ^{238}U$
E_{cm} = 892 MeV
ANGULAR MOMENTUM (ħ)
300
200
0
100
200
300
400
time (fm/c)

Figure 6

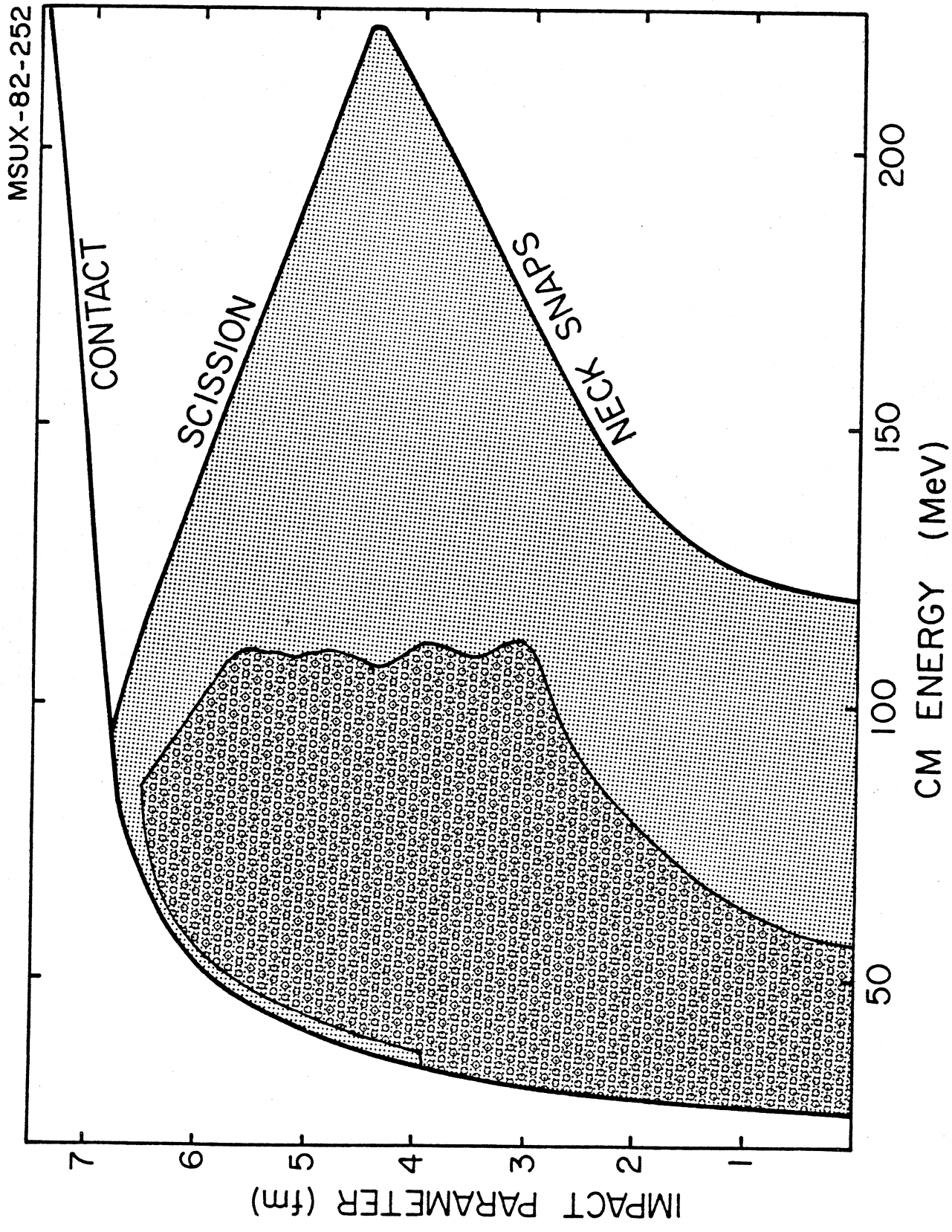
MSUX-82-252
CONTACT
SCISSION
NECK SNAPS
IMPACT PARAMETER (fm)
CM ENERGY (MeV)
1
2
3
4
5
6
7
50
100
150
200

Figure 7

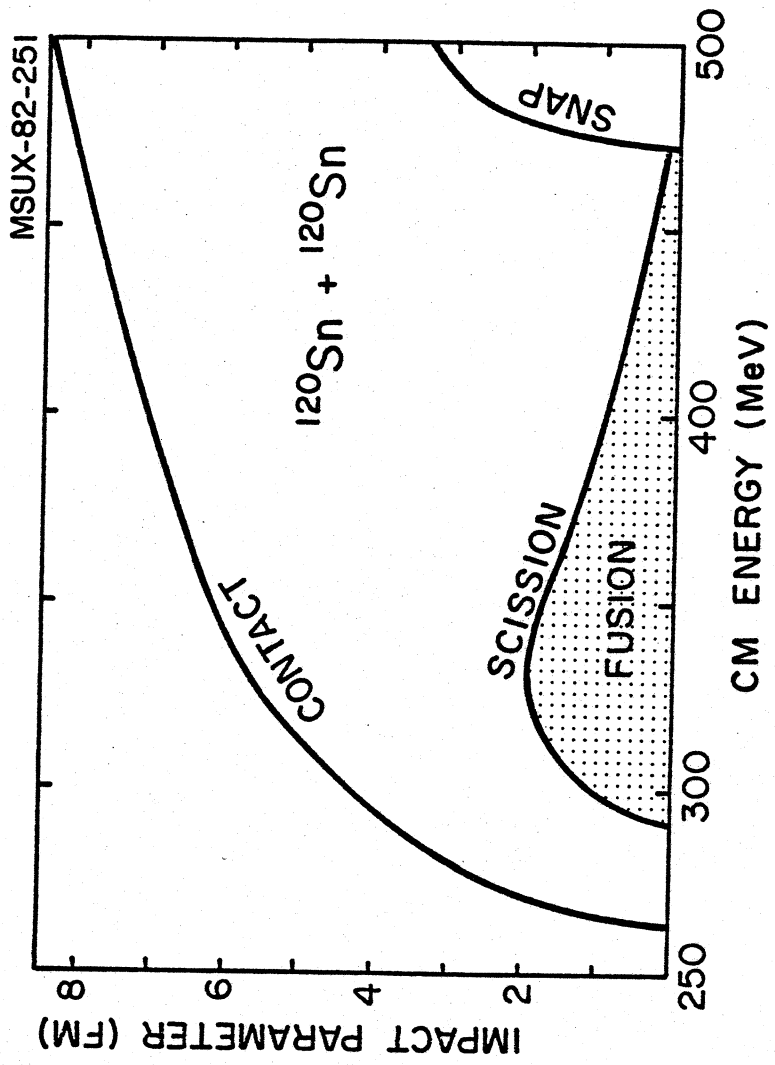
MSUX-82-251
$^{120}Sn + ^{120}Sn$
SNAP
CONTACT
SCISSION
FUSION
IMPACT PARAMETER (FM)
CM ENERGY (MeV)
8
6
4
2
500
400
300
250

Figure 8

Figure 9

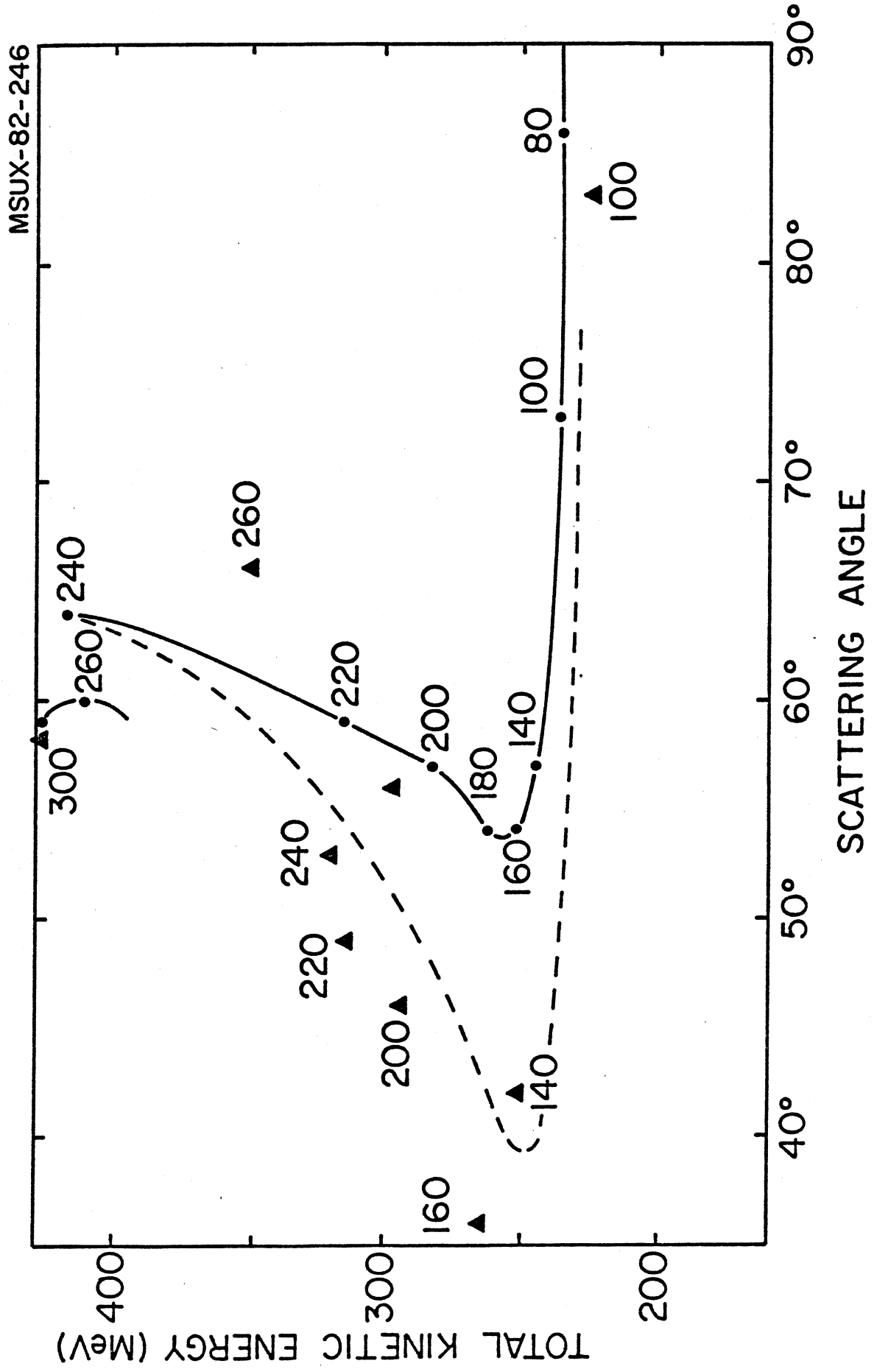
MSUX-82-246
TOTAL KINETIC ENERGY (MeV)
SCATTERING ANGLE
400
300
200
40°
50°
60°
70°
80°
90°
300
260
240
220
200
180
160
140
100
80
260
240
220
200
160
140
100